Received: 9 August 2018 | Revised: 25 April 2019 | Accepted: 1 May 2019
DOI: 10.1002/we.2358

WILEY

RESEARCH ARTICLE

Performance and wake of a Savonius vertical-axis wind turbine under different incoming conditions

Alexander D. Aliferis | Marius Stette Jessen | Tania Bracchi | R. Jason Hearst

Energy and Process Engineering, Norwegian University of Science and Technology, Trondheim, NO-7491, Norway

Correspondence
R. Jason Hearst, Energy and Process Engineering, Norwegian University of Science and Technology, Trondheim NO-7491, Norway.
Email: jason.hearst@ntnu.no

Abstract

In this study, the performance, drag, and horizontal midplane wake characteristics of a vertical-axis Savonius wind turbine are investigated experimentally. The turbine is drag driven and has a helical configuration, with the top rotated 180° relative to the bottom. Both performance and wake measurements were conducted in four different inflow conditions, using Reynolds numbers of $Re_D \approx 1.6\times10^5$ and $Re_D \approx 2.7\times10^5$ and turbulence intensities of 0.6% and 5.7%. The efficiency of the turbine was found to be highly dependent on the Reynolds number of the incoming flow. In the high Reynolds number flow case, the efficiency was shown to be considerably higher, compared with the lower Reynolds number case. Increasing the incoming turbulence intensity was found to mitigate the Reynolds number effects. The drag of the turbine was shown to be independent of the turbine's rotational speed over the range tested, and it was slightly lower when the inflow turbulence was increased. The wake was captured for the described inflow conditions in both optimal and suboptimal operating conditions by varying the rotational speed of the turbine. The wake was found to be asymmetrical and deflected to the side where the blade moves opposite to the wind. The largest region of high turbulent kinetic energy was on the side where the blade is moving in the same direction as the wind. Based on the findings from the wake measurements, some recommendations on where to place supplementary turbines are made.

KEYWORDS

drag, performance, turbulence, wake, VAWT

1 | INTRODUCTION

The world's demand for renewable energy is rapidly increasing. With the development of ''greener'' cities and the establishment of zero- and plus-energy buildings, this demand goes beyond large-scale electrical production systems such as offshore wind power and hydropower. The implementation of smart grid systems in cities and other densely populated areas comes with an expectation of more on-site electrical production systems. An alternative to the already well-developed and widely used rooftop photovoltaic systems is urban wind power. However, wind conditions in urban areas are highly variable, turbulent, and characterized by low mean velocities.[1] Thus, they are far from optimal for traditional horizontal-axis wind turbines (HAWTs). The performance of vertical-axis wind turbines (VAWTs) is, on the other hand, known to be less influenced by these environmental factors, leading to recent commercial investigation and development of VAWTs in the application of urban wind power. VAWTs are generally divided into two main groups, lift driven and drag driven. Within these two categories of turbines, the drag-driven Savonius turbine has the advantage of good self-starting abilities and peak performance at low rotational velocities, the latter adding the additional benefits of low noise emission and decreased risk of personal injury and property damage should a structural malfunction occur. While lift-type VAWTs also have their benefits, the present study will focus on Savonius-type turbines for these reasons.

There have been several papers published on the performance of Savonius turbines. Blackwell et al[2] found a Reynolds dependency of the turbine performance in wind tunnel experiments. Generally, the Reynolds number for VAWTs is given by

$$Re_D = \frac{\rho U_\infty D}{\mu}, \tag{1}$$

where ρ is the density, U_∞ is the incoming velocity, μ is the viscosity, and D the turbine diameter. Blackwell et al,[2] however, described their flow conditions with Reynolds number per meter [$Re = \rho U_\infty/\mu$], with values of 4.32×10^5 [1/m] and 8.67×10^5 [1/m]. They observed superior performance for their high Reynolds number cases compared with the low Reynolds number cases. A similar Reynolds dependency was reported by Damak et al[3] for a Savonius turbine with helical twist operating in a Reynolds number (Re_D) range of 7.97×10^4 to 1.47×10^5. The twisted configuration was also demonstrated to increase the efficiency by Saha and Rajkumar.[4] Akwa et al[5] presented a review of studies on Savonius rotors and stated that in addition to Re_D, the performance is also highly dependent on the aspect ratio, bucket spacing, bucket overlap, number of rotor stages, bucket and rotor geometry, shaft, and other accessories such as end plates. For example, both end plates and high aspect ratio are found to increase the performance by reducing the negative effects of a finite length turbine bucket.

In the investigation of VAWTs in urban environments, it is of great interest to map their performance in turbulent conditions. Loganathan et al[6] measured the effect of different turbulence intensities on the power output of a Savonius microturbine with 24, 30, and 40 blades operating under a range of wind speeds. The turbulence intensities ranged from 1.8% to 17%. There are few reports on similar experiments for more conventional two-bladed Savonius turbines, both with and without helical twist. Some comparable results have however been simulated by Akwa[7] using the finite volume method for turbulence intensities of 1% and 10%. All results show a negative impact on the performance with increasing turbulent intensity. These findings are interesting because they contrast with similar HAWT studies. As stated by Bardal and Sætran,[8] HAWT power output is increased with increasing turbulence intensity (TI) for operating conditions far below rated wind speed. The opposite trend was however found when the turbine operates in conditions closer to the rated wind speed. This concept is also supported by the equivalent power mathematics of Choukulkar et al[9] that suggest that an increase in TI can only increase the available power if operating below rated conditions. The conventional representation of performance is with the coefficient of power defined by

$$C_P = \frac{P}{\frac{1}{2}\rho A U_\infty^3}, \tag{2}$$

where P is the turbine output power and A is the projected frontal area of the turbine. Following Bardal and Sætran,[8] values of C_P will either increase or decrease with the TI. To exclude these dependencies, a turbulence equivalent wind speed, proposed by Choukulkar et al[9] and Wagner et al,[10] that considers the impact of shear, veer, and TI on the available energy in the incoming flow can replace U_∞ in Equation (2). Discussion of the Savonius turbines' power production in the context of an equivalent wind speed was not included in Loganathan et al[6] and Akwa,[7] nor in the review by Akwa et al.[5] The response of the Savonius turbine to wind gusts has, however, been evaluated by Marmutova,[11] who found that the performance dependency on tip-speed ratio was reduced with increasing gust frequency.

For structural considerations, it is important to investigate the drag force acting on the turbine. Fujisawa and Gotoh[12] analyzed the differences in drag force with respect to the tip-speed ratio; the latter is defined as

$$\lambda = \frac{\omega R}{U_\infty}, \tag{3}$$

where ω is the turbine rotational velocity and R is the radius of the turbine. They found the time-averaged drag on the Savonius turbine to be independent of the tip-speed ratio at values above 0.4. The experiments of Alder[13] support this conclusion. They also found that the drag coefficient given by

$$C_D = \frac{F_D}{\frac{1}{2}\rho A U_\infty^2}, \tag{4}$$

where F_D is the drag force, is approximately unity for Reynolds numbers between 2×10^5 and 6×10^5. Both of these studies are however limited to the case of low TI. Pol[14] has made a comparison of laminar and turbulent inflow conditions. The results are however obtained using computational fluid dynamics (CFD), for a single Reynolds number and a constant rotational speed of the turbine. The TI of the inflow is not specified. Nevertheless, Pol found that the drag coefficient decreases from 1.29 to 1.21 with an increase of the TI in the inflow. Thus, there are few existing measurements that investigate the drag characteristics of a Savonius turbine in different Reynolds number and turbulent inflow conditions, resulting in a gap in the literature.

Another important aspect in the urban application of vertical wind turbines is the development of the wake downstream of the rotor. Knowledge on the wake behavior is important for the arrangement of multiple turbines in limited space. It is also valuable in the optimization process of different blade configurations. Torresi et al[15] obtained the unsteady flow field for different angular positions downstream of a two-bladed Savonius rotor using hot-wire anemometry. They focused on blade optimization rather than turbine array configuration, so the wake measurements were bound to $x/D \lesssim 1.2$ (x being the streamwise coordinate) behind the rotor. In contrast, Shigetomi et al[16] examined the flow field around a single Savonius rotor as well as an array of two turbines for optimal configuration. They captured the flow field using particle image velocimetry and obtained values of both streamwise and cross-stream velocities up to $x/D \approx 3$. The results showed that there were four specific arrangements of the array that gave superior performance relative to that of a single turbine. The identified arrangements utilize the fact that the wake of a Savonius turbine is asymmetrical. By evaluating the frequency spectrum of streamwise velocity fluctuations, Shigetomi et al[16] found two evident peaks at frequencies equal to one and two times the cyclic frequency of the turbine. The peak at the lower of these frequencies was hypothesized as being a result of the shedding of a single vortex in a unit rotation of the turbine. The possible formation of a

staggered vortex street downstream of the turbine was also mentioned as a possible explanation for this lower peak, while the higher frequency peak was coupled to the passage of the two turbine "buckets." Further analysis on turbine interaction using CFD was done by Zhang et al[17] with an increased number of turbines and a more detailed investigation of the turbulent kinetic energy (TKE) in the wake. They found that one of the optimal array configurations identified by Shigetomi et al[16] was superior to the others. The optimal layout is achieved by placing downstream secondary turbines on the advancing blade side, outside the wake of prior turbines, making use of the wake asymmetry. The advancing blade is the blade moving in the same direction as the wind, while the returning blade moves towards the wind.

Reports on wakes in hydrokinetic applications of Savonius turbines also exist. Brammer et al[18] compared CFD results with experimental data for the average wake velocity of a Savonius tidal stream turbine. Their results showed good agreement between the simulated and measured values. A more comprehensive wake study for different Reynolds numbers with CFD, and some description of turbulent behavior in the wake, was reported by Kumar and Saini.[19] That work does however focus on the effects of twist angle on the overall performance and not on wake recovery. Each of these reports on hydrokinetic application of a Savonius turbine are only based on one constant value of TI of 10% and 5%, respectively.

In 2012, SINTEF[20] placed a number of helical Savonius turbines on one of Oslo's tallest buildings (Biskop Gunnerus Gate 14) to obtain correlations between wind measurements, electricity production, and noise. They concluded, among other things, that wake aspects of wind resources in the built environment are poorly understood and that further development work is necessary to exploit the full potential of Savonius turbines in an urban wind environment.

The present study aims to improve our understanding of the wake and aerodynamic performance of a Savonius wind turbine with low and high levels of incoming TI. This is in contrast to most previous studies that have been performed using a single level of TI for the inflow. Even though some of the studies have looked at the effects of turbulence on the power output and efficiency, they have not directly compared the Reynolds dependency with that of an approximately laminar inflow. In addition to the investigation of the wake with different initial flow conditions, the present study provides detailed analysis of the wake and its recovery under different operating conditions. This includes the assessment of turbulent momentum transport in the wake, which is a common way of assessing wake recovery for HAWTs and lift-type VAWTs,[21,22] but seemingly absent from the Savonius turbine literature. Furthermore, the present study is also intended to give perspective on the turbine interaction results from Zhang et al[17] with different incoming flow conditions. As flow in an urban environment is highly turbulent, and turbulent flow conditions are known to change both the drag and wake characteristics of bodies in general,[23,24] the robustness of the optimal configuration suggested by Zhang et al[17] must be assessed.

To perform the aforementioned analysis, all components of the wake velocity in the horizontal plane have been measured using two dynamic four-hole pressure probes traversed in the range $1.12 \leq x/D \leq 11.6$ downstream of the turbine. The two chosen Reynolds numbers for measurements of both performance and wakes in this study are based on results of C_P-dependency on Reynolds number found in preliminary measurements. For wake measurements, two different λ were chosen to represent optimal and suboptimal operating conditions of the turbine.

2 | EXPERIMENTAL DETAILS

2.1 | Wind tunnel and turbine

The experiments were conducted in the low-speed closed-loop wind tunnel in the Fluid Mechanics Laboratory at the Norwegian University of Science and Technology. The test section of the wind tunnel is 11 m long, 2.71 m wide, and 1.81 m high. To counteract wall boundary layer growth, the height of the ceiling is gradually increased to 1.85 m through the test section. This wind tunnel has been used in numerous previous small-scale and model wind turbine studies, eg, Bartl and Sætran.[25]

The Savonius turbine used in this study is a single unit from the commercially available 150 W TurboMill system by WindStream Technologies. Only a single rotor from the system, which originally included three VAWTs, was used, and the driving and housing structures in the present study were built in-house and are described in greater detail below. Thus, the results presented herein do not, and are not meant to, represent or reflect on the commercially available system. Instead, this rig is meant to gain insight on the behavior of VAWTs in different incoming conditions in general. The turbine has a helical twist where the top is rotated 180° relative to the bottom as depicted in Figure 1. It is also equipped with end plates. The turbine has diameter $D = 0.33$ m, is 0.99 m tall, and has a projected frontal area of $A = 0.327$ m^2. For all measurements, the turbine was placed 4.5 m (13.6D) downstream of the test section inlet, as shown in Figure 2, which includes additional information about the experimental setup.

With the turbine inside the tunnel, the blockage is 9.86%. Velocities are corrected for the blockage effect of the turbine using Pope and Harper's correction method[26]:

$$U_c = U_\infty \left(1 + \frac{A}{4A_t}\right), \tag{5}$$

where A is the model blocked area and A_t the wind tunnel area.

FIGURE 1 Savonius wind turbine used in the present experiment. Additional support struts connecting support structure to the ceiling are visible [Colour figure can be viewed at wileyonlinelibrary.com]

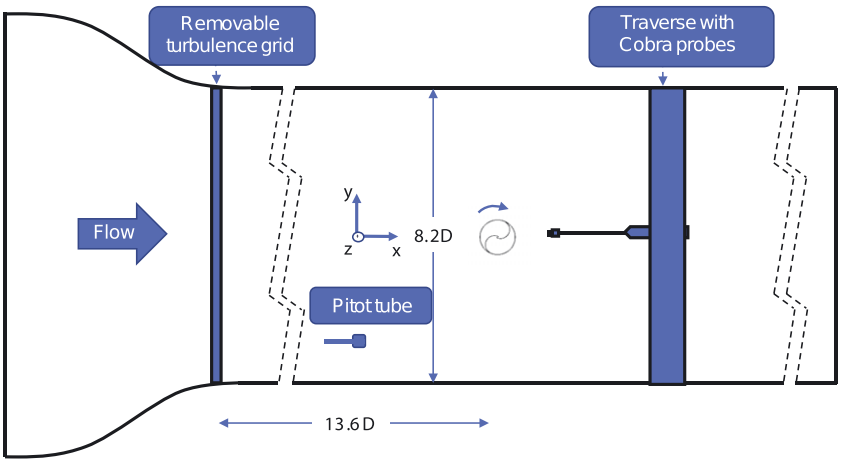

FIGURE 2 Schematic of the experimental setup in the wind tunnel. View is from above [Colour figure can be viewed at wileyonlinelibrary.com]

2.2 | Inflow conditions

Turbine performance and wake characteristics were investigated for four different inflow conditions. The conditions were changed by having either an approximately laminar or fully turbulent inflow and using two different Reynolds numbers: $Re_D \approx 1.6 \times 10^5$ and $Re_D \approx 2.7 \times 10^5$, which correspond to mean incoming velocities of $U_\infty \approx 7.8$ m/s and $U_\infty \approx 13.9$ m/s, respectively. The Reynolds numbers selection was based on preliminary results of uniform flow measurements on the same turbine conducted by the authors. These measurements exhibited high Reynolds number dependence for Reynolds numbers between 0.86×10^5 to 2.61×10^5. Reynolds numbers above 2.61×10^5 resulted in negligible changes in the measured nondimensionalized performance.

The velocity vector is decomposed into three velocity components where U is the velocity in the x-direction (streamwise), V in the y-direction (cross-stream), and W is the velocity component in the z-direction (vertical). In order to analyze the turbulent statistics of the flow, all of the velocity components are further broken down such that

$$U = \langle U \rangle + u'; \quad V = \langle V \rangle + v'; \quad W = \langle W \rangle + w', \tag{6}$$

where, U, V, and W are the instantaneous total velocities, $\langle U \rangle$, $\langle V \rangle$, and $\langle W \rangle$ are the time-averaged (mean) velocities, and u', v', and w' are the time-varying velocity fluctuations. By defining the velocity in this manner, the streamwise TI may be defined as

$$I = \frac{\sqrt{\langle u'^2 \rangle}}{\langle U \rangle}. \tag{7}$$

FIGURE 3 View of the setup inside the wind tunnel looking upstream. *Left:* Uniform inflow with additional support struts connecting the turbine to the ceiling. *Right:* Turbulent inflow with grid at the inlet of the test section [Colour figure can be viewed at wileyonlinelibrary.com]

TABLE 1 Summary of inflow conditions [Color table can be viewed at wileyonlinelibrary.com]

Test Case Number	Turbulence Grid	Reynolds Number Re_D	Turbulence Intensity $I[\%]$
1	No	1.6×10^5	0.6
2	No	2.7×10^5	0.6
3	Yes	1.5×10^5	5.7
4	Yes	2.7×10^5	5.7

Note. When the turbulence grid was used, it was placed at the inlet of the test section and the turbine was placed $x = 4.5$ m $= 13.6D = 18.4M_g$ downstream

The TI of the incoming flow is varied by placing a turbulence-generating grid at the inlet of the wind tunnel, as illustrated in Figure 3. The grid is made of wooden bars with 47 mm × 47 mm cross section. The mesh length of the grid is $M_g = 0.245$ m, resulting in a solidity of 35%. Introducing the grid to the flow induced some variations in the horizontal velocity profile of the incoming flow; however, the variation over the turbine diameter was within 1.5% peak to peak. Similar observations were made by Bartl and Sætran[25] who used the same grid. The different inflow conditions, measured at the model location with the tunnel empty, are summarized in Table 1.

2.3 | Performance measurements

The turbine power production can be calculated from $P = M \cdot \omega$, where M is the torque produced by the turbine and ω is the rotational velocity of the turbine. The produced torque, M, was measured using a Hottinger Baldwin Messtechnik GmbH (HBM) torque transducer (type T20W-N/5-Nm). The rotational velocity, ω, was found by measuring the number of turbine revolutions per minute (RPM), n, with an optical RPM sensor and the relation $\omega = 2\pi n/60$. A Siemens three-phase squirrel-cage motor with rated power of 550 W was used as a generator in the experiments. This is fundamentally the same setup as Bartl and Sætran[25] but reoriented for a VAWT instead of an HAWT. The schematic of the turbine setup is shown in Figure 4.

For the power and drag coefficients estimate from Equations (2) and (4), respectively, the density is calculated from the ideal gas law using the temperature measured with a thermocouple. The incoming velocity is calculated from the dynamic pressure, measured with a pitot-static tube placed ahead of the turbine. As a result of calculating the power from the torque ($P = M \cdot \omega$), the torque coefficient is $C_M = C_P/\lambda$ and thus contains no additional information; therefore, focus is placed on C_P and C_D only as they are independently measured. In an effort to reduce the influence of considerable vibrations in the system, the turbine was attached to the ceiling with additional support struts during the C_P measurements.

The drag force is measured using the streamwise-aligned load cell on the wind tunnel's six-component force balance (produced by Carl Schenck AG). Again, this component has been used in previous experiments at the same facility.[25] In order to remove the drag force contribution from the support structure, the drag force was measured under all inflow condition without the turbine. The drag force of the turbine itself was then isolated as $F_D = F_{D_{total}} - F_{D_{support}}$. Additional supports to the ceiling were not used for the drag measurements because all force must be transmitted through the force balance.

For all performance measurements, the sampling rate was 1000 Hz and the sampling time was 30 seconds. The performance of the turbine was captured in all flow conditions by varying the turbine rotational speed using the mentioned Siemens induction motor controlled by a frequency converter. The energy generated by the turbine was dissipated in a small electric heater.

2.4 | Wake measurements

The wake behind the turbine was measured using two Cobra probes produced by Turbulent Flow Instrumentation (TFI). Cobra Probes are four-holed dynamic pressure probes, capable of measuring all three velocity components and local static pressure in real time. These probes were

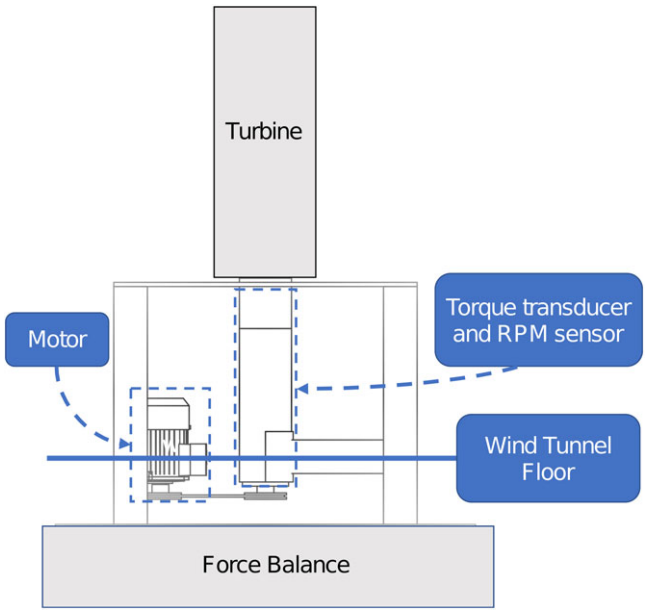

FIGURE 4 Schematic of the turbine setup in the wind tunnel, as seen from the side. Schematic is not to scale [Colour figure can be viewed at wileyonlinelibrary.com]

also used to measure the incoming velocity profiles and turbulence intensities for the empty tunnel. For all the wake measurements, the turbine was mounted to the ceiling.

Figure 5 illustrates the measurement grid. The grid is uniformly spaced in the span with $\Delta y = 3$ cm between each measurement point. There are 15 such scans distributed downstream of the turbine, with the last measurements at $x/D = 11.6$. The necessary grid spacing was found by performing an initial scan and investigating the resolution of the velocity components. In the z-direction, the measurement plane was located at the center of the turbine height. The sampling frequency was 1250 Hz for all wake measurements, which was sufficient to capture the first- and second-order velocity statistics. For the measurements at the lowest Reynolds number, the sampling time was 60 seconds while a sampling time of 30 seconds was used for the highest Reynolds number. The reasoning behind lowering the sampling time at higher Reynolds number is that as the velocity increases, so does the eddy-turnover time. Thus, in order to measure a similar number of eddy turnovers for fair comparison, the sampling time is reduced when the velocity is increased. Some longer measurements of 120 seconds were taken in locations of high turbulence for spectral analysis.

The wake behind the turbine was captured under the four inflow conditions described in Table 1 and two different operating conditions. These test cases were chosen in order to isolate the effects of Reynolds number, tip-speed ratio, and TI. The operating condition of the turbine was altered by changing the tip-speed ratio of the turbine. A summary of the different wake test cases is provided in Table 2. For all cases, the integrated bulk velocity across the span at the first streamwise position ($x/D = 1.12$), referred to as U_0, is used for normalizing the velocity. This quantity is conserved through the flow and as such is a representative velocity for comparison between cases.

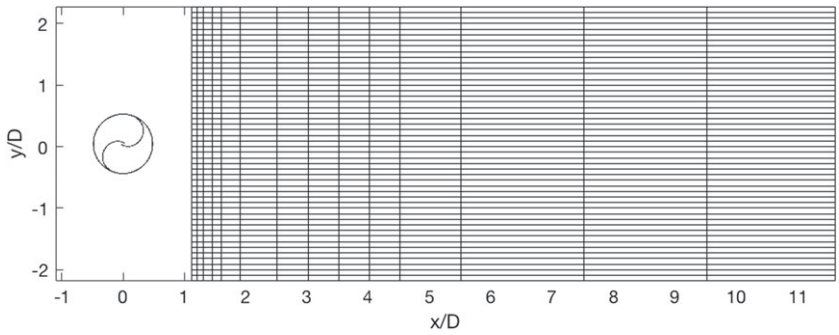

FIGURE 5 Measurement grid seen from above. Here, x is the distance from the turbine center in the streamwise direction and y is the horizontal cross-stream direction. $y = 0$ represents the center of both the turbine and the wind tunnel

TABLE 2 Flow and turbine parameters for the wake measurements

Test Case Number	Turbulence Grid	Reynolds Number Re_D	Tip-speed Ratio λ
A	No	1.7×10^5	0.8
B	Yes	1.7×10^5	0.8
C	No	2.7×10^5	0.8
D	Yes	2.8×10^5	0.8
E	No	1.7×10^5	0.4
F	Yes	1.6×10^5	0.4

2.5 | Measurement uncertainties

The uncertainties in the measurements of performance were calculated as described by Wheeler.[27] Random statistical errors are computed for a 95% confidence interval for all measured parameters. Systematic errors originating from the calibration procedures are also accounted for. The total error in each measured variable is calculated as the root sum square of the random and systematic errors.

For each of the calculated variables C_P, C_D, and λ, the error is found by the law of error propagation using the total error in each dependent parameter. All performance variables are plotted with their respective uncertainties, and the mean relative error of each measurement series is presented as well.

The accuracy of the Cobra probes is quoted from the manufacturer to be dependent on the turbulence level. Generally, it should be within ±0.5 m/s and ±1° in pitch and yaw angles (used to calculate velocity components) up to about 30% TI. The conditions in this study are generally well below this limit, and thus, the uncertainty is below the aforementioned values. In regions of very high TI, ie, near the turbine, the accuracy of the measurements is somewhat lower. Draskovic[28] investigated the accuracy of these probes compared with laser Doppler anemometry and hot wire anemometry and concluded that the Cobra probes were suitable for measurements in complex turbulent flows. The measured error in mean velocities at 10 m/s and high ambient turbulent conditions was about 2%. Furthermore, the maximum error in TI was 1%, but in most cases, it was not more than 0.6%. The quoted accuracy from the manufacturer together with the stated errors by Draskovic[28] make the Cobra probes suitable for the experiments reported herein.

Measurements in the wind tunnel without the turbine but with the turbulence generating grid showed that the TI decays from 5.7% to 3.3% from $x/D = -2$ to $x/D = 11.6$. The decay of turbulence in the longitudinal direction of a wind tunnel is a well-documented phenomenon and is reported here only for reference, cf, Comte-Bellot and Corrsin,[29] Hearst and Lavoie,[30] and Lavoie et al.[31]

3 | WIND TURBINE PERFORMANCE

3.1 | Power coefficient

The power coefficient, C_P, was calculated as per Equation (2) using the measured average torque and the blockage corrected velocity. Averaged values of the coefficient of power, C_P, and their associated uncertainties are plotted in Figure 6 for the described inflow conditions. By inspecting the figure, an increase in both the magnitude and the tip-speed ratio of the maximum power coefficient $C_{P_{max}}$ for increasing Re_D is evident. This is quantified in Table 3. The impact of increased TI appears to reduce C_P for the higher Re_D case but not the lower one. Considering this from a different perspective, for the same change in Re_D, the maximum power coefficient changes by a smaller amount in a turbulent flow compared with an approximately laminar flow. A quantifiable example of this is C_P at $\lambda = 0.7$ that grows by 48% when Re_D is increased from 1.6×10^5 to 2.7×10^5 in the low turbulence case but grows by only 44% for the high turbulence case. Interestingly, when the proposed equivalent wind

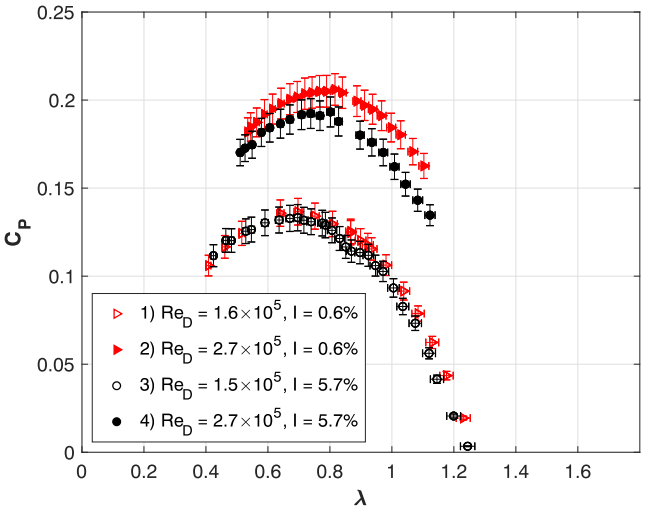

FIGURE 6 Power coefficient, C_P, as a function tip-speed ratio, λ, for the Savonius turbine. Plotted with uncertainties in both variables [Colour figure can be viewed at wileyonlinelibrary.com]

TABLE 3 Max power coefficient and mean drag coefficient for different performance test cases

Test Case		Inflow Conditions		Power Coefficient		Drag Coefficient	
#		Re_D	I[%]	C_{Pmax}	Mean Error	$C_{D_{mean}}$	Mean Error
1	▷	1.6×10^5	0.6	0.137	±3.4%	1.15	±8.9%
2	▶	2.7×10^5	0.6	0.207	±4.3%	1.15	±6.0%
3	○	1.5×10^5	5.7	0.134	±4.4%	1.11	±10.4%
4	●	2.7×10^5	5.7	0.194	±4.4%	1.09	±6.5%

Note. The listed uncertainties are the average of the uncertainty at every measurement position for a given test case.

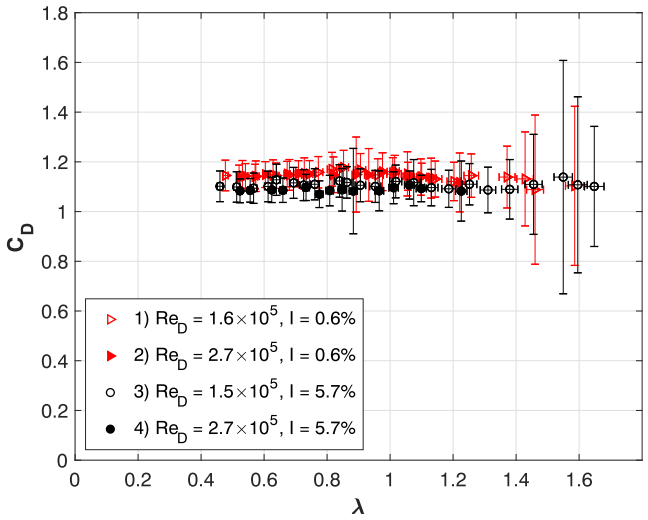

FIGURE 7 Drag coefficient, C_D, as a function tip-speed ratio, λ, for the Savonius turbine with uncertainties in both variables [Colour figure can be viewed at wileyonlinelibrary.com]

speed of Choukulkar et al[9] is used in the calculation of C_P and λ, no significant change is observed in Figure 6.

Blackwell et al,[2] who experimented on conventional Savonius turbines, suggested that the observed Reynolds number dependence is due to delay of flow separation for high Re_D on the convex side of the rotor buckets, induced by the transition to a turbulent boundary layer. This phenomenon is especially significant when the rotor has an angular position near 0° and 180° (ie, the edge of either bucket is facing the incoming flow). At these angles, the flow characteristics on the facing bucket are similar to flow around a cylinder. When the boundary layer becomes turbulent and separation is delayed, the pressure drag on the returning bucket is reduced. This is because of the increased pressure recovery on the concave side of the bucket. As the pressure drag on the returning bucket at those angular positions reduces, the torque is increased. Because the turbine in question has a helical twist, there are more angular positions in a rotation where a "bucket" is facing the wind. We therefore suspect that the helical geometry increases the effect described above, causing an even stronger Reynolds number dependence. This idea is supported by the fact that the data obtained by Blackwell et al[2] on conventional Savonius turbines with no helical twist show a weaker Reynolds number dependence than that observed here. Damak et al,[3] who performed experiments on a Savonius turbine with an helical twist, also observed a stronger Reynolds number dependence compared with the study by Blackwell et al.[2] A summary of the maximum value and the mean error of the power coefficient for all four cases is summarized in Table 3. The values of $C_{P,max}$ are consistent with the upper range of those reported by Akwa et al.[5] Resulting uncertainties are also quite low and in agreement with uncertainties obtained by Blackwell et al.[2]

3.2 | Drag Coefficient

Figure 7 depicts the drag coefficient, C_D, as a function of tip-speed ratio for the Savonius turbine. Here, the measured drag force is normalized as per Equation (4) and adjusted for the drag of the support structure. The drag coefficient appears to be independent of λ. This is supported by drag measurements from other Savonius experiments, eg, Fujisawa and Gotoh,[12] who found that C_D only varies significantly for $\lambda < 0.4$, thus leading to their hypothesis that blade blockage effects are the dominant source of drag force on Savonius turbines. Blade blockage is simply the effect of solid blades preventing the flow from passing through the turbine's swept area, which results in an increased drag force when the turbine rotates faster. As the Savonius turbine has very small gaps where air can pass through it, this blockage effect can reach a maximum value at quite low rotational speeds. The uncertainty in the drag coefficient for high λ is large in the present study due to increased vibrations at high rotational speeds.

Averaged values of C_D over the tested λ-ranges are summarized in Table 3. The values of C_D are similar between Reynolds numbers, but a slight decrease is observed for highly turbulent inflow. We note that this small deviation is within our uncertainty margins; however, the existence of a decrease in C_D for increasing TI (within the range tested here) is corroborated by other studies. For instance, Pol[14] performed CFD analysis on a Savonius turbine using both laminar and turbulent simulation models and reported similar findings. This phenomenon may perhaps be explained by comparing the results to the familiar case of a cylinder in cross flow. A previous study performed by Bell[32] showed that increasing the TI in the incoming flow up to 5% induces reduction in C_D for a cylinder. This is because the intensity of perturbations in the boundary layer increases, causing the separation points to move backwards and reducing the pressure drag. A similar effect may act on a Savonius turbine as well.

4 | WAKE MEASUREMENTS

4.1 | Velocity deficit

The normalized time-averaged streamwise velocity, $\langle U\rangle/U_0$, is illustrated in Figure 8. For all cases, there is a highly visible velocity deficit behind the turbine. This deficit is skewed towards $y/D < 0$, resulting in an asymmetric wake. Asymmetric wakes for VAWTs are well documented by

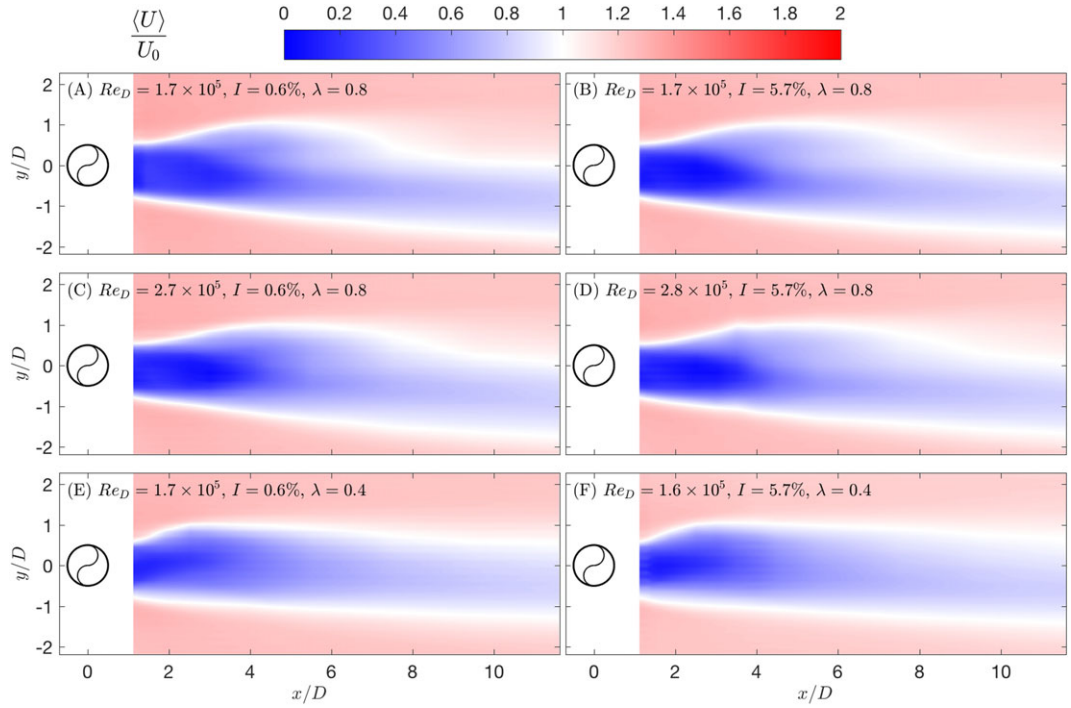

FIGURE 8 Contours of normalized time-averaged streamwise velocity of the wake in the *xy*-plane. The area shown in each plot is equivalent to that of the measurement grid depicted in Figure 5 [Colour figure can be viewed at wileyonlinelibrary.com]

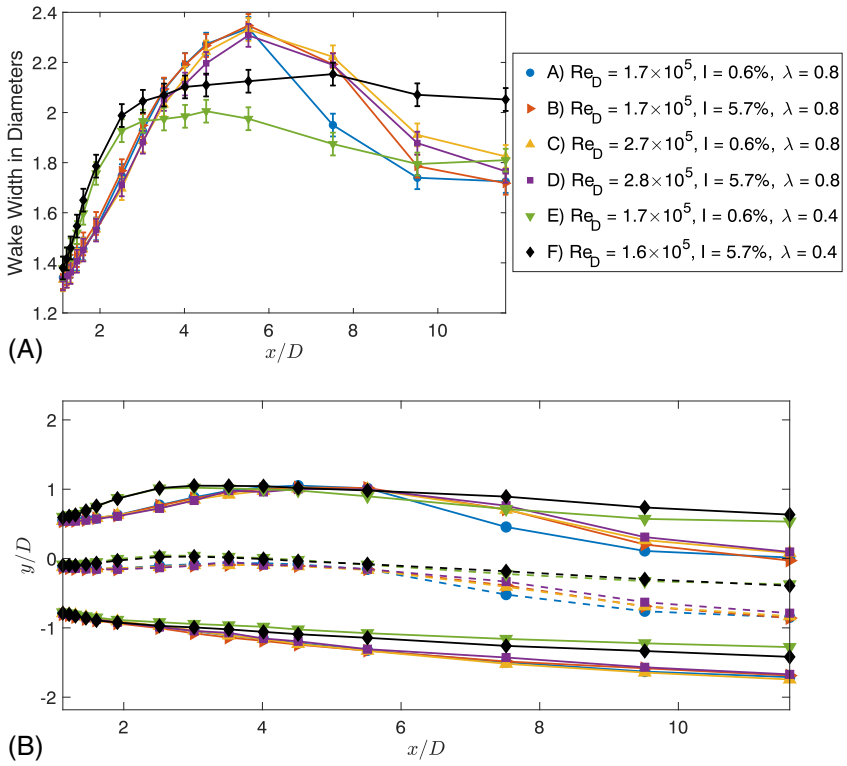

FIGURE 9 A, Development of the wake thickness, ie, the distance between lines of $\langle U\rangle/U_0 = 1$ in the wake. B, Contours of $\langle U\rangle/U_0 = 1$ for all test cases. The dashed lines depict the centerline of the wake. In (B), the size of the symbols represent the uncertainty [Colour figure can be viewed at wileyonlinelibrary.com]

previous studies on drag-driven Savonius turbines, eg, Zhang et al,[17] and lift-driven Darrius turbines, eg, Shamsoddin and Porté-Agel[21] and by Hohman et al.[33] Generally, the wake is asymmetric because the returning blade of the VAWT is a more significant obstruction to the incoming flow than the advancing blade. Shigetomi et al[16] also linked asymmetrical wake behavior to a Magnus effect created by the vertical rotation of the turbine. For ease of discussion, regions of $y/D < 0$ and $y/D > 0$ will hereafter be referred to as the strong and weak side of the wake, respectively. The wake width is explicitly depicted in Figure 9, where there are large deviations between the different types of inflow and operating conditions. In the low Reynolds numbers cases, the wake is wider for high incoming TI, at least in the downstream region $5.5 < x/D \lesssim 11$ for optimal λ and $x/D > 2$ for suboptimal λ. This is in contrast to results from experiments on HAWTs obtained by Tian et al,[22] where high inflow turbulence gave a

narrower wake than the case of low inflow turbulence for $Re_D = 9 \times 10^4$. At suboptimal operating conditions, ie, low λ, the increase in wake width with TI is highest and exists farther downstream of the rotor. This can be explained by the airflow on the turbine blades having more similarities with airflow on a sharp-edged disc when the relative velocity of the turbine to the incoming flow is reduced. Rind and Castro[23] reported that the boundary layer separation point on a sharp edged disc remains unchanged with inflow TI and that stronger TI increases the disc wake deficit and

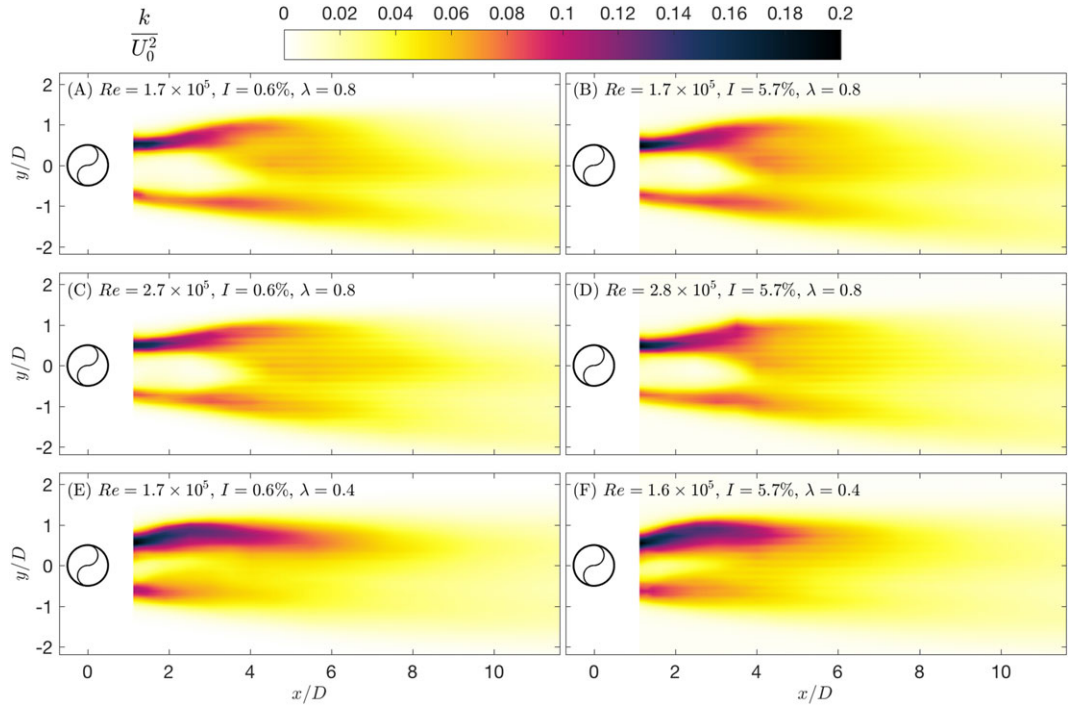

FIGURE 10 Contours of normalized time-averaged turbulent kinetic energy, *k*, in the *xy*-plane of the wake [Colour figure can be viewed at wileyonlinelibrary.com]

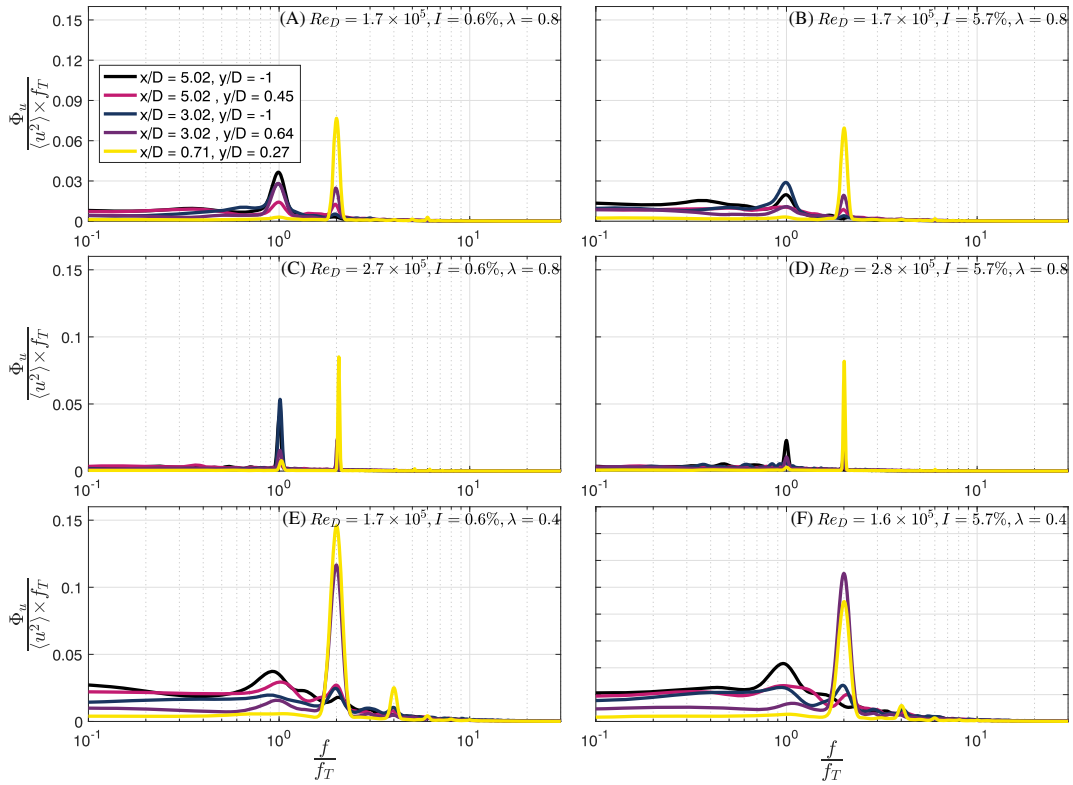

FIGURE 11 Normalized streamwise velocity fluctuation spectrum at several downstream positions for each test case [Colour figure can be viewed at wileyonlinelibrary.com]

width. This is in contrast to flow around a sphere or cylinder where stronger TI delays separation and hence reduces the wake deficit and width. For higher Reynolds numbers, the aforementioned relation between TI and wake width is reversed over the tested range of x/D, and there is less variation with differing incoming TI, suggesting that the impact of TI for increasing Re_D is diminished.

4.2 | Wake turbulence

The TKE in the wake is given by

$$k = \frac{1}{2}\left[\langle u'^2\rangle + \langle v'^2\rangle + \langle w'^2\rangle\right] \tag{8}$$

and is depicted in Figure 10. For all cases, the TKE is highest in the region behind the advancing turbine blade. This result can be related to more powerful vortex shedding from the tip of the advancing blade as can be seen in the spectra reported in Figure 11, which is discussed further in the next section.

The TKE on the strong side of the wake is lower in the high Re_D cases. The reduction in the peak value of TKE with respect to increased Reynolds number is 8.28% and 9.27% for the cases of low and high TI, respectively. Schaffarczyk et al[34] found that flow separation increases production levels of TKE. Thus, the explanation of increased efficiency due to less flow separation on the returning blade for higher Reynolds number is in good agreement with this observed reduction of TKE. Comparing the results of different inflow TI, the spatial distribution of large TKE levels seems to increase for high TI. These larger values are especially evident towards the centerline, $y/D = 0$. The peak values of TKE are, however, more or less unchanged.

In the wind turbine wake literature, it is common to investigate the turbulent momentum fluxes as they quantify flow entertainment into the wake. Figure 12 shows the normalized values of the Reynolds shear stress, $\langle u'v'\rangle$, which represents the lateral momentum flux for the different cases. For all cases, there are two regions, one of positive and one of negative flux, that transfer energy from the outer flow into the wake. The levels of these entrainments are however quite dependent on the tip-speed ratio. Near the optimal operating conditions of $\lambda = 0.8$, the momentum flux on the weak side of the wake is dominant. The highest levels of entrainment in the strong side of the wake is also farther downstream. Interestingly, in the near wake ($x/D < 4$), the entrainment from the strong side extends less towards the middle for case (A) than in the other cases. To quantify this, the measured turbulence momentum flux in case (B), which has the second lowest value at $(x/D, y/D) = (3.5, 0.36)$, is 107% larger than in case (A). This is in agreement with the centerline of the wake in case (A) depicted in Figure 9B, being more deflected towards the strong side. The mentioned effect of less entrainment in this region is delayed in terms of $\langle U\rangle$ and is hence observable farther downstream, eg, $x/D > 6$. The absolute values of turbulent momentum flux are almost equal in magnitude, and despite the described deviation above, the fluxes in the near wake are very similar regardless of the Reynolds number. With lower operating λ, the levels of entrainment become more evenly distributed, which results in a more symmetric wake. The most evident difference created by the increased levels of TI is in the farthest regions of the wake ($x/D > 8$), especially on the weak side. The lateral span of this region is increased by about 10% to 20% between the different cases for increased levels of inflow turbulence. By the lower black contour line in Figure 12, it is also observable that there is a small increase in the lateral

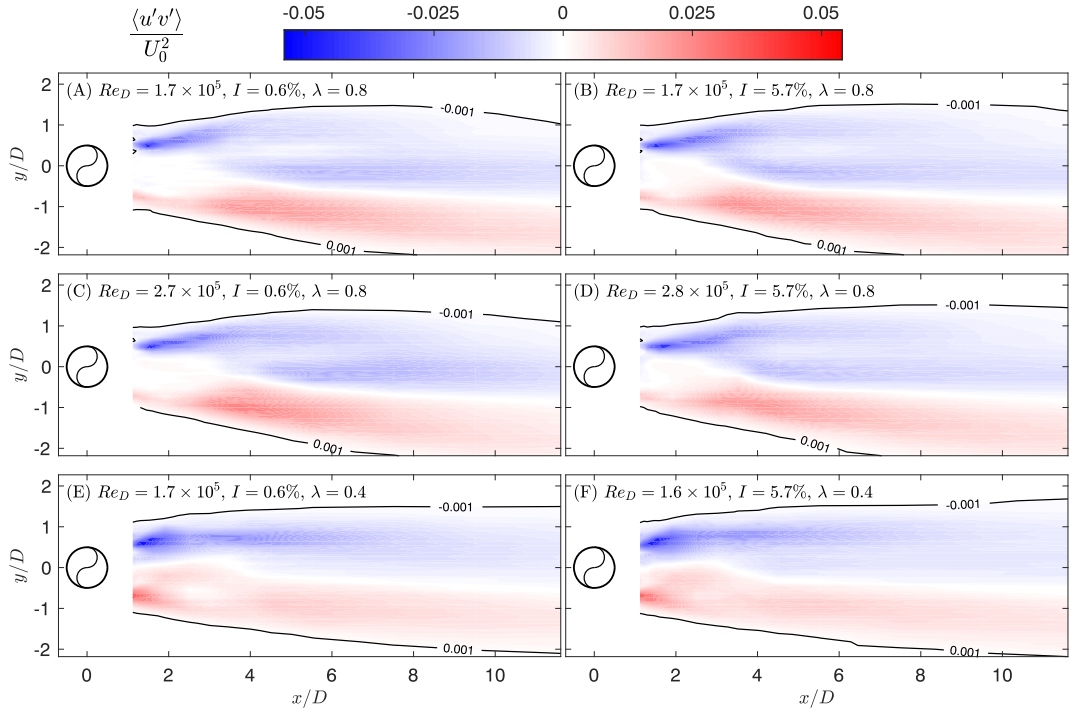

FIGURE 12 Normalized contours of lateral momentum flux $\left(\langle u'v'\rangle/U_0^2\right)$ in the wake of the turbine for all cases [Colour figure can be viewed at wileyonlinelibrary.com]

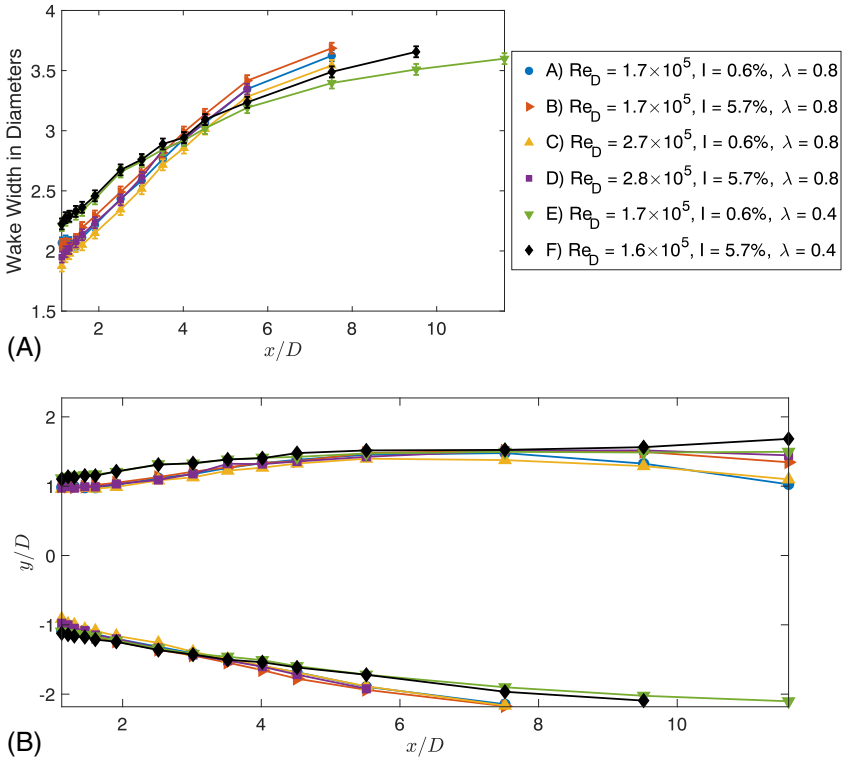

FIGURE 13 A, Development of Reynolds shear stress wake thickness, ie, the distance between lines of $|\langle u'v'\rangle/U_0^2| = 0.001$. B, Contours of $|\langle u'v'\rangle/U_0^2| = 0.001$ for all test cases. In (B), the size of the symbols represent the uncertainty [Colour figure can be viewed at wileyonlinelibrary.com]

span of entrainment on the strong side of the wake as well. Figure 13 depicts the width between the entrainment levels of −0.001 and 0.001 in the outer region of the wake for the different cases. The effect of larger entrainment regions in the far wake with high inflow TI is relatable to the development in wake width of the mean velocity field as shown in Figure 9A. The difference in wake width in the case of suboptimal λ is reduced in this same region. Thus, increased inflow TI induces a higher rate of wake recovery for all cases in the far wake, due to more turbulent mixing with high TI. This can be substantiated by the slope of the curves for high inflow TI in Figure 9A, being negative for $x/D > 9$.

5 | TIME SERIES ANALYSIS

Shigetomi et al[16] proposed that vortex streets exist in the wakes of Savonius wind turbines. Their study does, however, only consider a limited number of measurement points and no different inflow conditions. In the present study, positions used in the spectral analysis of streamwise velocity fluctuations are chosen to map any development of such a vortex street in different inflow conditions and to compare points of high and low time-averaged TKE to the vortex shedding from the two turbine blades. The normalized results are given in Figure 11, where $f_T = n/60$.

Similar to Shigetomi et al,[16] there are two spectral peaks at frequencies of one and two times the turbine rotation rate. The latter peak is a result of the two-bladed structure of the turbine, as a point in the circumference is passed twice by a blade per unit rotation. The inner peak suggests that a single vortex is shed once during a complete rotation. This peak could also be related to the formation of a vortex street behind the turbine. These two peaks appear in all test cases; thus, their existence appears to be independent of the tested incoming conditions. The CFD of Frikha et al[35] suggests that the vortex shedding from the returning and advancing blade does not coincide. The collision and interaction of these vortices shed at different positions can thus produce a staggered vortex street in the wake. The fact that the observed inner peak is most noticeable and of greater magnitude for $x/D > 1.41$ is in good agreement with the possible formation of a vortex street and hence the concept promoted by Shigetomi et al.[16]

It should be kept in mind that the different operating conditions induce differences in the characteristics of the wake. As seen in Figure 10, the spatial distribution of TKE and hence peak fluctuations are different for the given inflow conditions. This redistribution is obvious when comparing results in the spectra for different operating tip-speed ratios, as the strongest fluctuations are measured farther downstream in the wake for the reduced λ. By the point-wise spectrum representation in Figure 11, it is difficult to identify specific effects of increased TI and Reynolds number. In some instances, values are reduced. In others, values are increased. Nonetheless, they clearly identify that there are two dominant frequencies in the wake flow, which is suggestive of both vortex shedding, and a combined effect of multiple shedding mechanisms.

6 | CONCLUSION

This study has reported measurements of the aerodynamic performance and wake evolution of a Savonius wind turbine at two Reynolds numbers and two turbulence intensities. Similar to Akwa et al,[5] results show that the power coefficient decreases with higher inflow TI. This decrease was

however only observable for the highest Reynolds number. Thus, the Re_D-dependence of the power coefficient is reduced as the turbulence is increased. The drag coefficient showed little dependence on λ, and a slight decrease was found for higher inflow TI. This finding is also supported by the earlier CFD simulations performed by Pol.[14] When considered in the context of a cylinder in a high TI flow, this effect can possibly be related to less flow separation around the turbine.

The detailed wake measurements in the different operating conditions described above revealed that the wake was asymmetric. Time-averaged analysis indicates that the largest velocity deficit occurs behind the returning turbine blade. The measured asymmetry was noticeably dependent on λ, and the largest asymmetry was observed for the case of low Reynolds number and TI. In contrast to the results of HAWTs, the wake width of the Savonius turbine was found to increase with low Reynolds number and turbulent inflow. The opposite effect was however observed for high Reynolds number. This was linked to the evolution of lateral turbulent momentum flux, which drives the wake recovery.

Finally, considering the results presented herein, it is possible to give some insight on the optimal placement of supplementary Savonius turbines. Due to the blockage of incoming wind by the first rotor, there are two downstream regions of high time-averaged streamwise velocities outside the wake. As the wake is asymmetric, the accelerated region behind the advancing blade is the sensible position given that this allows for turbines to be placed closer together. To get the most out of the blockage effect, a second turbine should not be placed too far downstream either. Although previously believed to increase overall efficiency, placement of a second turbine with the returning blade in the strong side wake of the upstream turbine was proven to be inefficient by Zhang et al.[17] They proposed a different layout where the second turbine is placed outside the upstream turbine wake, providing an accelerated incoming velocity profile similar to that of the leading turbine. Zhang et al[17] suggested that this should be at $(x/D, y/D) \approx (5.8, 2.4)$. This recommendation is echoed here, with the further comment that this position appears to be relatively robust to different turbulence intensities, Reynolds numbers, and tip-speed ratios.

ACKNOWLEDGEMENTS

The authors thank A.E. Kolstad, A. Brandastrø, and B. Brandastrø for their aid in preparing, maintaining, and problem solving the experimental setup. The authors are also grateful to L.M. Bardal for his help with the data acquisition systems and Getek AS in Trondheim for donating the Savonius turbine.

ORCID

R. Jason Hearst https://orcid.org/0000-0003-2002-8644

REFERENCES

1. Kumara E, Hettiarachchi N, Jayathilake R. Review paper: Overview of the vertical axis wind turbines. *International Journal of Scientific Research and Innovative Technology*. 2017;4:2313-3759.
2. Blackwell BF, Sheldahl RE, Feltz LV. Wind tunnel performance data for two- and three-bucket Savonius rotors; 1978. Tech. rep., Sandia Laboratories, Sand 76-0131 under act AT/29-11 Page 789.
3. Damak A, Driss Z, Abid M. Experimental investigation of helical Savonius rotor with a twist of 180 degrees. *Renewable Energy*. 2013;52:136-142.
4. Saha U, Rajkumar MJ. On the performance analysis of Savonius rotor with twisted blades. *Renewable Energy*. 2006;31:1776-1788.
5. Akwa JV, Vielmo HA, Petry AP. A review on the performance of Savonius wind turbines. *Renewable and Sustainable Energy Rev*. 2012;16:3054-3064.
6. Loganathan B, Mustary I, Chowdhury H, Alam F. Effect of turbulence on a Savonius type micro wind turbine. *Energy Procedia*. 2017;110:549-554. 1st International Conference on Energy and Power, ICEP2016, 14-16 December 2016, RMIT University, Melbourne, Australia.
7. Akwa JV. Análise aerodinâmica de turbinas eólicas Savonius empregando dinâmica dos fluidos computacional. Master's Thesis, Universidade Federal do Rio Grande do Sul. Escola de Engenharia. Programa de Pós-Graduaação em Engenharia Mecânica; 2010.
8. Bardal LM, Sætran LR. Influence of turbulence intensity on wind turbine power curves. *Energy Procedia*. 2017;137:553-558.
9. Choukulkar A, Pichugina Y, Clack CTM, Calhoun R, Banta R, Brewer A, Hardesty M. A new formulation for rotor equivalent wind speed for wind resource assessment and wind power forecasting. *Wind Energy*. 2016;19:1439-1452.
10. Wagner R, Antoniou I, Pedersen SM, Courtney MS, Jørgensen HE. The influence of the wind speed profile on wind turbine performance measurements. *Wind Energy*. 2008;12:348-362.
11. Marmutova S. Performance of a Savonius wind turbine in urban sites using CFD analysis. Ph.D. Thesis, University of Vaasa Faculty of Technology Energy Technology P.O. Box 700 FI-65101 Vaasa Finland; 2016.
12. Fujisawa N, Gotoh F. Experimental study on the aerodynamic performance of a Savonius rotor. *J Sol Energy Eng*. 1994;116:148-152.
13. Alder G. The aerodynamic performance of the Savonius rotor. In: 2nd Int. Symp. on Wind Energy Systems, Amsterdam, the Netherlands; 1978(2)E10:119-126.
14. Pol PAM. Numerical study of flow through a Savonius wind turbine. Bachelor's thesis, Grau en Enginyeria en Vehicles Aeroespacials, Universitat Politècnica de Catalunya; 2015.
15. Torresi M, Benedittis FAD, Fortunato B, Camporeale SM. Performance and flow field evaluation of a Savonius rotor tested in a wind tunnel. *Energy Procedia*. 2014;45:207-216. ATI 2013 - 68th Conference of the Italian Thermal Machines Engineering Association.
16. Shigetomi A, Murai Y, Tasaka Y, Takeda Y. Interactive flow field around two Savonius turbines. *Renewable Energy*. 2011;36:536-545.
17. Zhang B, Song B, Mao Z, Tian W. A novel wake energy reuse method to optimize the layout for Savonius-type vertical axis wind turbines. *Energy*. 2017;121:341-355.
18. Brammer J, Falconer R, Kwan A. Physical and numerical modelling of the wake characteristics of the Savonius tidal stream turbine. In: Proceedings of 2013 IAHR Congress. At: Chengdu, China; 201309.

19. Kumar A, Saini R. Performance analysis of a Savonius hydrokinetic turbine having twisted blades. *Renewable Energy*. 2017;108:502-522.
20. Haase M, Skeie KS, Tronstad TV. Building integrated vertical wind turbines : experiences from the roof of biskop gunnerus gate 14 in Oslo. *SINTEF Fag*. 2014.
21. Shamsoddin S, Porté-Agel F. Large-eddy simulation of atmospheric boundary-layer through a wind farm sited on topography. *Boundary-Layer Meteorol*. 2017;163(1):1-17. https://link.springer.com/article/10.1007/s10546-016-0216-z
22. Tian W, Ozbay A, Hu H. Effects of incoming surface wind conditions on the wake characteristics and dynamic wind loads acting on a wind turbine model. *Phys Fluids*. 2014;26:125108.
23. Rind E, Castro IP. On the effects of free-stream turbulence on axisymmetric disc wakes. *Exp Fluids*. 2012;53:301-318.
24. Hearst RJ, Gomit G, Ganapathisubramani B. Effect of turbulence on the wake of a wall-mounted cube. *J Fluid Mech*. 2016;804:513-530.
25. Bartl J, Sætran L. Blind test comparison of the performance and wake flow between two in-line wind turbines exposed to different turbulent inflow conditions. *Wind Energy Sci*. 2017;2:55-76.
26. Ross IJ. Wind tunnel blockage corrections: an application to vertical-axis wind turbines. Master's Thesis, University of Dayton; 2010.
27. Wheeler AJ, Ganji ARG. *Introduction to engineering experimentation*. 3rd ed.: Pearson Education; 2004. Chap. 7.
28. Draskovic N. Measurement methods in turbulent flows. Master's Thesis, Norwegian University of Science and Technology; 2017.
29. Comte-Bellot G, Corrsin S. The use of a contraction to improve the isotropy of grid-generated turbulence. *J Fluid Mech*. 1966;25:657-682.
30. Hearst RJ, Lavoie P. Decay of turbulence generated by a square-fractal-element grid. *J Fluid Mech*. 2014;741:567-584.
31. Lavoie P, Djenidi L, Antonia RA. Effects of initial conditions in decaying turbulence generated by passive grids. *J Fluid Mech*. 2007;585:395-420.
32. Bell W. The influence of turbulence on drag. *Ocean Eng*. 1979;6:329-340.
33. Hohman T, Martinelli L, Smits A. The effects of inflow conditions on vertical axis wind turbine wake structure and performance. *J Wind Eng Ind Aerodyn*. 2018;183:1-18.
34. Schaffarczyk A, Pawlak M, Richert F. New model for calculating intensities of turbulence in the wake of wind-turbines. In: Proceedings - DEWEK 2002, 6th German Wind Energy Conference; Wilhelmshaven, Germany; 2002:18-21.
35. Frikha S, Driss Z, Kchaou H, Abid MS. Incidence angle effect on the turbulent flow around a Savonius Wind Rotor. *Am J Energy Res*. 2016;4:42-53. https://doi.org/10.12691/ajer-4-2-3

How to cite this article: Aliferis AD, Jessen MS, Bracchi T, Hearst RJ. Performance and wake of a Savonius vertical-axis wind turbine under different incoming conditions. *Wind Energy*. 2019;1–14. https://doi.org/10.1002/we.2358